

Mathematical Models for Current, Voltage, and Coupling Capacitor Voltage Transformers

Working Group C-5 of the Systems Protection Subcommittee of the IEEE Power System Relaying Committee, Demetrios A. Tziouvaras, *Chairman*, Peter McLaren, *Vice Chairman*, George Alexander, Douglas Dawson, Jules Esztergalyos, Charles Fromen, Mietek Glinkowski, Irwin Hasenwinkle, Mladen Kezunovic, Ljubomir Kojovic, Bill Kotheimer, Richard Kuffel, Jerry Nordstrom, and Stanley Zocholl

Abstract—This paper reviews a number of mathematical models used to represent the nonlinear behavior of the magnetic core of instrument transformers. Models of instrument transformers using these core representations are presented. The transient response of the instrument transformer is compared to actual test results recorded in the laboratory. The paper provides practical guidelines as to which of the physical elements of instrument transformers are important to model during transient studies and which elements could be ignored without sacrificing the accuracy of the simulation results. The electromagnetic transients program (EMTP) data files used to generate the models are also provided in the appendix to help new EMTP users model instrument transformers for evaluation of high-speed protective relaying systems.

Index Terms—Coupling capacitor voltage transformers, current transformers, EMTP modeling, simulation, voltage transformers.

I. INTRODUCTION

ELECTRIC power systems are subjected to many types of disturbances that result in electrical transients due to lightning, faults or routine operations such as line energization and deenergization, opening of disconnects, and switching of inductive or capacitive loads.

When a sudden change occurs, such as a system fault, a redistribution of the electric and magnetic energy stored in the capacitive and inductive elements of the network must occur due to the dynamics of the power system. This redistribution of energy cannot occur instantaneously and the power system must go through a transient state before it reaches a new steady state.

During the first few cycles following a power system fault, high-speed protective relays are expected to make a correct decision as to the presence and location of the fault in order to preserve system stability and to minimize the extent of equipment damage. The majority of protective relays make their decisions based on 50 and 60 Hz fundamental frequency voltage and current signals. However, it is precisely at this moment that the voltage and current signals are badly corrupted by fault induced transients in the form of an exponentially decaying dc component and with frequencies above and below the fundamental power system frequency.

The dynamic performance of high-speed protective relays depends to a large extent on the signals produced by the instrument transformers, and these signals depend on the overall transient

response of the instrument transformers and the type of transients generated by the power system.

The transient performance of current transformers (ct) is influenced by a number of factors with most notable the exponentially decaying dc component of the primary current. Its presence influences the build-up of core flux, a phenomenon which is likely to cause saturation and subsequently substantial errors in the magnitude and phase angle of the generated signals. The core flux is composed of an alternating and a unidirectional component corresponding to the ac and dc components of the primary fault current. The transient flux swing generated by the dc component of the primary fault current can be quite large compared to the one created by the ac component. The ct core may also retain an unknown amount of flux, because of the ferromagnetic character and whether or not the ct has antiremanence air gaps. This remanent flux will either aid or oppose the build-up of core flux and could contribute to ct saturation, during subsequent faults in the power system such as high-speed autoreclosing into a permanent fault, depending on the relative polarities of the primary dc component and the remanent flux. Furthermore, after primary fault interruption, the ct could still produce a unipolar decaying current due to the stored magnetic energy.

The transient response of magnetic voltage transformers (vts), and coupling capacitor voltage transformers (ccvts) depends on several distinct phenomena taking place in the primary network such as, sudden decrease of voltage at the transformer terminals due to a fault, or sudden overvoltages on the sound phases caused during line to ground faults on the network. Sudden decrease of voltage at the primary terminals could generate internal oscillations in the windings of magnetic vts which creates a high frequency on the secondary side. These high frequency oscillations are typically damped within 15–20 ms. However, in the case of ccvt, energy stored in the capacitive and inductive elements of the device generate transients with low frequency of aperiodic character which could last up to 100 ms. Sudden increase of voltage at the primary terminals of magnetic vts could cause saturation of the magnetic core.

The transient errors produced by the instrument transformers can have a major impact on the dependability and security of the protective relays and cause either misoperations, delayed operations, or failures to operate. Fault induced transients and transients generated by the measuring transformers make the study of relay system performance for h.v. and e.h.v. networks based on fundamental frequency inadequate.

The use of electromagnetic transient programs to adequately model the different power system components and to generate transient data to assess the performance of modern high-speed protective relays have become essential.

II. MATHEMATICAL MODELS OF MAGNETIC CORE REPRESENTATION

Models for instrument transformers are especially important for studying ct saturation, ferroresonance phenomena, harmonics, and subharmonics and their effect on the performance of protective relaying. The major nonlinear effects in iron cores are saturation, eddy currents, and hysteresis. The predominant effect in cts is saturation, whereas the predominant effect in cvts and vts is saturation and ferroresonance.

The working group reviewed a number of iron core models described in the literature and their summary is described below:

A. EMTP and ATP Inductor Models

The EMTP and alternative transients program (ATP) support two classes of nonlinear elements, a true nonlinear model (Type-93), and two pseudo-nonlinear models (Type-96 and Type-98). In the true nonlinear model the nonlinearity of the element is explicitly defined as a nonlinear function, i.e., the flux ψ as a function of the current ($\psi = f(i)$). The EMTP and ATP then solve the combination of nonlinear equations and an appropriate system equivalent at each time step using a Newton-Raphson iterative procedure.

In the pseudo-nonlinear model, the nonlinearity is defined as a number of piece-wise linear segments. Such linear segments are represented by the program with a resistor in parallel with an appropriate current source. In the particular case of a nonlinear inductor, the flux is monitored at each time step in order to determine which linear segment should be used to compute the inductance at that time step. Note that this methodology does not model the true nonlinearity since the program relies on previous time step results to decide on what segment to operate next. The EMTP and ATP change segments only after they have operated illegally outside the range of the current segment. It is therefore important to use a small time step during the simulation so that the operating point moves up and down the nonlinearity in small increments.

EMTP and ATP support the following two additional magnetic saturation routines:

- Subroutines CONVERT (in EMTP) and SATURATION (in ATP) are designed to convert rms $v-i$ saturation curve data into peak $\psi-i$ data with the hysteresis loop being ignored.
- Subroutines HYSDAT (in EMTP) and HYSTERESIS (in ATP) are designed to provide the hysteresis loop data required by the Type-96 pseudo-nonlinear reactor model.

This model uses data points from the ct secondary excitation curve, $V_{\text{rms}} - I_{\text{rms}}$, as inputs to subroutine CONVERT to obtain data points of peak flux, ψ , versus peak current i . The result is a piece-wise linear model because a small finite number of data points are used, usually 10 or less.

The peak $\psi-i$ data are computed from the rms saturation curve voltage and current values [1]. The conversion of rms

voltage values to flux is only a rescaling procedure. For each linear segment in the $\psi-i$ curve,

$$\psi_k = \frac{\sqrt{2}V_k}{\omega} \quad (1)$$

where ω is the angular frequency.

For the first linear segment in the $\psi-i$ curve,

$$I_1 = I_{1-\text{rms}}\sqrt{2}. \quad (2)$$

Assuming that $\psi_k(\theta) = \psi_k \sin \theta$, then for the following segments ($k \geq 2$), the peak current is obtained by evaluating $I_{k-\text{rms}}$ for each segment k , using (3) given in [1]

$$I_{k-\text{rms}}^2 = \frac{2}{\pi} \left(\int_0^{\theta_1} \left(\frac{\psi_k \sin \theta}{L_1} \right)^2 d\theta + \int_{\theta_1}^{\theta_2} \left(I_1 + \frac{\psi_k \sin \theta - \psi_1}{L_2} \right)^2 d\theta + \dots + \int_{\theta_{k-1}}^{\pi/2} \left(I_{k-1} + \frac{\psi_k \sin \theta - \psi_{k-1}}{L_k} \right)^2 d\theta \right). \quad (3)$$

In (3) only the last segment L_k is unknown. Equation (3) can be rewritten in the form

$$a_{lk}Y_k^2 + b_{lk}Y_k + c_{lk} = 0 \quad (4)$$

with constants a_{lk} , b_{lk} , and c_{lk} known, and $Y_k = 1/L_k$ to be computed. Y_k can then be solved from (4) and it must be positive. The peak current i_{lk} is computed from

$$i_k = i_{k-1} + Y_k(\psi_k - \psi_{k-1}). \quad (5)$$

One point from the $\psi-i$ curve is inputted in the subroutine HYSDAT which then generates the major hysteresis loop data. This routine contains predefined trajectories in the $\psi-i$ plane to decide which path to follow when the flux increases or decreases.

A resistance in parallel with the inductor is used to represent core losses due to eddy currents. Other elements also represented are the primary and secondary resistances and leakage reactances, and the secondary burden resistance and reactance.

These EMTP/ATP models allow the user to represent the effects of residual flux left in the ct following primary current interruption. They can also be easily integrated directly into EMTP/ATP power system studies. Finally because the model parameters are derived from ct test data, a degree of validity is implied.

The main disadvantage is the need to preprocess the data points from the ct excitation curve to generate the data for the Type-96 hysteretic reactor model.

B. EMTDC Model

This model represents the magnetizing branch of the transformer equivalent circuit as a nonlinear inductor in parallel with a nonlinear resistor [4], [5]. The current in this branch has two components, i_m and i_c , the magnetizing current and the hysteresis current. The magnetizing current is described by a power series equation. The hysteresis current is described by an exponential equation using the Steinmetz coefficient of the core

material. In a variant of this model, terms are added to i_c to represent eddy current and other effects.

The coefficients of the power series for i_m are derived from the saturation curves for the transformer by an iterative calculation that produces a curve relating instantaneous flux and current values.

The resulting equations produce a smooth continuous $B-H$ loop representation similar to EMTP/ATP. This model also requires preliminary calculations using the ct saturation curve data to determine the power series coefficients.

Fig. 1 shows the equivalent circuit for the magnetizing branch of the transformer consisting of a nonlinear inductor in parallel with a nonlinear resistor.

The majority of electromagnetic transient programs use the Dommel algorithm [3] whereby inductances and capacitances are represented by a conductance in parallel with a current source. Nonlinear elements are represented by piece-wise linear conductances, however, this has the disadvantage of requiring reevaluation of the overall system conductance matrix at any time step when the solution calls for a change from one section to the next in the piece-wise linear conductance. The reevaluated conductance matrix has to be inverted adding yet further computational penalties. Avoiding matrix inversion is a worthwhile practice. In EMTDC the nonlinearity of both elements in Fig. 1(a) is combined into a voltage/current relationship as shown in Fig. 1(b). The eddy current loss resistor is constant for the frequency range of interest and is not included in the current source. Therefore, the current source contains the magnetizing current component i_m and a hysteresis component i_c .

The magnetizing current component is related to the core flux ψ by the equation

$$i_m = \sum k_j \psi^{a_j} \quad (6)$$

where k_j and a_j are both positive for all j [4]. Typically three terms of the power series give a very good fit to the measured curve over a wide range of values.

The hysteresis component i_c is of the form

$$i_c = k_h v^{\beta-1} \quad (7)$$

where k_h is a constant and β is the Steinmetz coefficient for the material. Constant k_h is in general frequency dependent but has been set for these studies to a value appropriate for 60 Hz. The total current source is therefore given by

$$i = i_m + i_c. \quad (8)$$

The voltage v across the current source i is computed from the flux ψ as

$$v = \frac{d\psi}{dt}. \quad (9)$$

It is also convenient to have i_m expressed in terms the reluctance \mathcal{R} and the number of secondary turns N_2

$$i_m = \frac{\mathcal{R}}{N_2} \psi \quad (10)$$

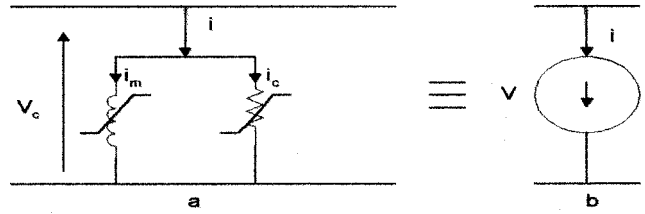


Fig. 1. Equivalent circuit and current source for the magnetizing branch.

and \mathcal{R}/N_2 can therefore be put in the form

$$\frac{\mathcal{R}}{N_2} = \sum k_j \psi^{a_j-1}. \quad (11)$$

In order to use (6) and (7) it is necessary to know v and ψ . The value of the current source i injected into the network will in turn affect the value of v depending on the network source impedance as seen from the terminals of this current source and the magnitude of i in comparison to the other currents flowing in the network. Voltage v and current i cannot be calculated independently of each other and an exact solution will require an iterative technique which adjusts v until the calculated value of i injected into the network, along with currents from all other sources, results in the same value of v . An iterative technique slows the simulation and in the case of real time digital simulators other algorithms have to be used to reduce the time of the simulation [5], [7].

C. "Seetee" Model

In this model the incremental permeability of the core material, $\mu_0\mu_r = dB/dH$, is obtained by taking the derivative of the Frolich equation [11]. The permeability is calculated at each time step to vary the nonlinear magnetizing inductance, L_m , in response to the core flux density. When the core flux density reaches a value which causes the $\mu_r = 1$ the permeability is fixed at this level until the flux density is again reduced. The result is a smooth single-valued anhysteretic curve relating the core flux density B to the magnetizing force H .

Although this model does not simulate a multivalued $B-H$ loop, comparison with full scale test data on saturating cts have shown excellent agreement in the waveforms produced. This suggests that the multivalued aspect of the hysteresis loop may have only a minor influence on the distortion of ct secondary currents.

Only two data points on the core are needed for the Frolich equation coefficients. These are, μ_m , the maximum core relative permeability, and B_{sat} , the saturation flux density. The nonlinear inductance L_m , represents the varying magnetizing inductance of the ct core during large current excursions. L_m is calculated from the relation:

$$L_m = \mu_0\mu_r N_2^2 A_c \frac{1}{L_c} \quad (12)$$

where:

- μ_r Relative maximum incremental permeability of the core material. For silicon steel it ranges from 2000–5000.
- μ_0 Permeability of free space $4\pi E - 7$ H/m.

- N_2 Number of ct secondary turns.
 A_c Cross sectional area of the ct core in m².
 L_c The mean length of the flux path in m.

The variable core permeability is the slope of the B/H curve at any specific point:

$$\mu_0\mu_r = \frac{dB}{dH}. \quad (13)$$

The ct model needs a defined relationship between B and H so that the permeability can be calculated. The Frolich equation can be used. One form of the equation is:

$$B = \frac{H}{c + b|H|} \quad (14)$$

where b and c are constants determined from the core material. The core permeability is expressed by:

$$\mu_0\mu_r = \frac{dB}{dH} = \frac{(1 - b|B|)^2}{c}. \quad (15)$$

When the core flux density reaches the saturation flux density, B_{sat} , the relative permeability of the core approaches unity. This provides one condition for defining how the constants b and c are related. For silicon steel B_{sat} is about 1.8 Tesla.

The maximum slope of the B/H curve occurs at $B = 0$ where the curve crosses the H axis. This is the maximum permeability of the core material, μ_m , and is a known constant. Therefore setting $B = 0$ in (15) and solving for c :

$$c = \frac{1}{\mu_0\mu_m}. \quad (16)$$

Using this value of c and letting $B = B_{sat}$, the constant b is obtained by:

$$b = \frac{1 - 1/\sqrt{\mu_m}}{B_{sat}}. \quad (17)$$

Using these constants the Frolich equation now defines the B/H curve between $B = 0$ and $B = B_{sat}$. The model disregards the equation for flux densities greater than B_{sat} and sets the permeability to μ_0 .

The model is based on several assumptions listed below. Due to extremely large excursions of the core flux it turns out these assumptions have negligible effect on the accuracy of the results. The assumptions of the model are:

- The B/H curve is assumed to be single valued. This is the same as assuming that the B/H curve has no area.
- The maximum permeability of the core occurs at $B = 0$. For most magnetic materials the permeability is low at low values of H , rises quickly to a maximum as H increases, and then gradually decreases at large values of H approaching that of free space at extreme values of H .

These assumptions limit the application of this model to large flux excursions caused by high currents. The results of this model may not be very accurate for very low currents.

D. Jiles–Atherton Model

This model is based on current physical theories of magnetic domains in ferromagnetic materials [9], [10]. It uses a Langevin

expression to generate an anhysteretic $M-H$ curve. This expression is used in a state equation to simulate the effects of domain wall bending and translation, i.e., reversible and irreversible domain wall motion, thereby modeling $M-H$ curves. The expression used for the anhysteretic $M-H$ curve is:

$$M(H) = M_s \left\{ \coth \left(\frac{H + \alpha M(H)}{a} \right) - \frac{a}{H + \alpha M(H)} \right\} \quad (18)$$

where

- M_s saturation magnetic moment of the core material,
- H magnetization force in the core,
- α interdomain coupling factor,
- A thermal energy parameter,
- m magnetic moment.

The equation for the contribution of the reversible domain wall motion to the core magnetization is:

$$\frac{dM_{rev}}{dH} = c \left(\frac{dM_{an}}{dH} - \frac{dM}{dH} \right) \quad (19)$$

where

- M_{an} anhysteretic magnetic moment,
- c domain flexing parameter.

For the irreversible wall motion the equation is:

$$\frac{dM_{irr}}{dH} = \left(\delta \frac{k}{\mu_0} - \alpha(M_{an} - M_{irr}) \right)^{-1} (M_{an} - M_{irr}) \quad (20)$$

where

- δ directional parameter, +1 for $dH/dt > 0$ and -1 for $dH/dt < 0$,
- μ_0 permeability of free space,
- k domain pinning parameter.

Combining (18)–(20) yields the total equation:

$$\frac{dM}{dH} = \frac{1}{1+c} \left(\delta \frac{k}{\mu_0} - \alpha(M_{an} - M) \right)^{-1} \cdot (M_{an} - M) + \frac{c}{1+c} \frac{dM_{an}}{dH}. \quad (21)$$

Using the expression for the anhysteretic moment given in (18) for M_{an} , the equation can be solved for the core magnetic moment as a function of H . However, this is a static solution and does not model the dynamic losses of the core material. Therefore the model includes a damping influence of the domain wall motion given by:

$$\frac{dM}{dt} = \gamma(b(H) - M(t)) \quad (22)$$

where γ is the domain damping parameter.

Given the magnetizing force as a function of time, $H(t)$, numerical integration techniques are used to solve (18), (21), and (22) simultaneously to obtain the core flux values at specified times.

Other core parameters that are needed to model a transformer core using this method are the magnetic cross section of the core, the magnetic path length, and the core stacking factor for laminated cores.

The various core hysteresis parameters required in this model, α , a , c , k , and δ can be calculated from experimental measurements of the coercivity, remanence, saturation flux density, initial anhysteretic susceptibility, initial normal susceptibility, and the maximum differential susceptibility. The domain damping parameter γ is derived from widening of the dynamic B - H loop with frequency.

Some commercially available programs use the Jiles-Atherton model to simulate the dynamic behavior of magnetic devices. An example of a B - H loop for a commercial 1200/5 current transformer core calculated by using one of these programs is shown in Fig. 2. In this simulation a sinusoidal current was used to excite the secondary winding with the primary open circuited. The current starts at zero and continues for 2.5 cycles. The initial magnetization curve can be seen to progress into a cyclical B - H loop. The secondary excitation current was 3.53 A rms.

The following parameters were used in the simulation shown in Fig. 2.

Secondary turns	240
Core area	2 sq. in.
Magnetic flux path length	39.4 in.
Core stacking factor	0.95
α Interdomain coupling	$9.5E-5$
a Thermal energy factor	100 A/m
B_{sat} saturation flux density	1.8 T
c domain flexing factor	0.07
γ domain damping factor	$1E+7$
k domain pinning parameter	150 A/m
μ_0 permeability of free space	$4\pi E-7$ H/m.

Equations other than Langevin's have been used for the anhysteretic B - H curve in the Jiles-Atherton model. Two examples are:

$$M_{an} = M_s \frac{M(H)}{|M(H)| + 1} \quad (23)$$

and

$$M_{an} = M_s (\tanh(M(H))). \quad (24)$$

Jiles-Atherton models based on (18) are sometimes referred to as Level 1 and those based on (23) are called Level 2. One commercially available simulation program allows a choice of Levels 1 or 2. However, the model using Level 2 does not include the interdomain coupling and damping effects. It is better suited to model ferrite and powdered iron cores than Level 1 and is more efficient in the calculation.

III. CURRENT TRANSFORMER MODEL

The transient response of cts and the correct ct models in an EMTP simulation are very important in the evaluation of high-speed relaying systems.

A. Equivalent Circuit

A reasonably accurate equivalent circuit of a ct up to a few kHz is shown in Fig. 3 with all quantities referred to the sec-

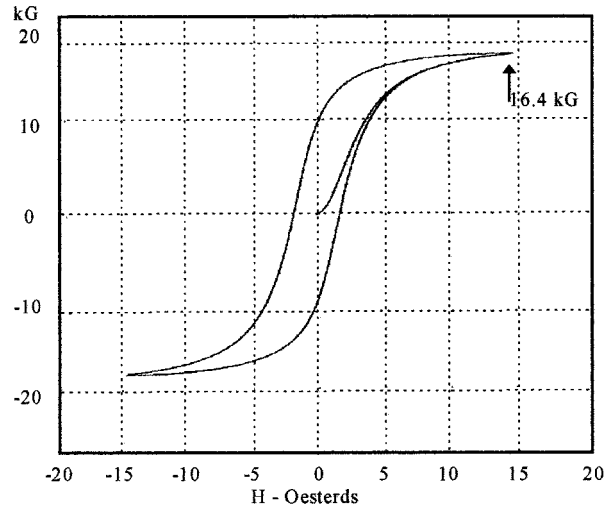


Fig. 2. B - H loop for the core of a 1200/5 current transformer simulated by the Jiles-Atherton method.

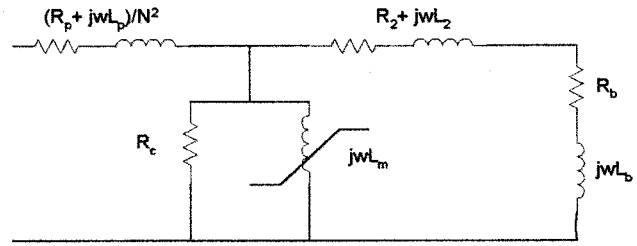
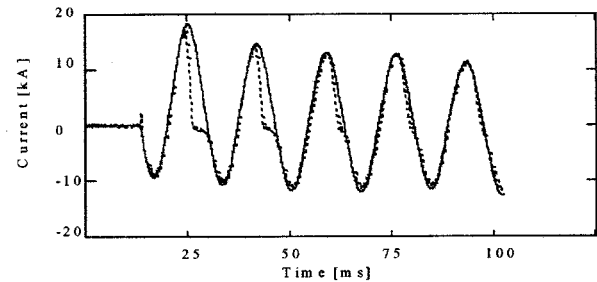
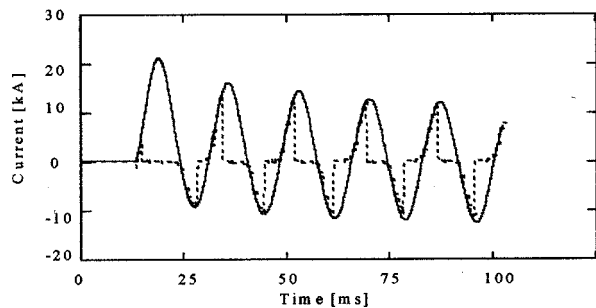


Fig. 3. Equivalent circuit of a ct.



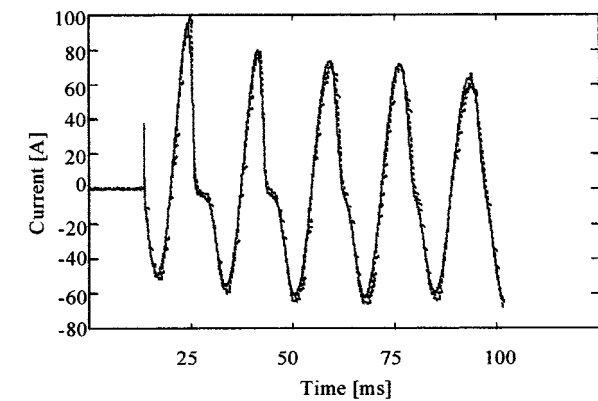
(a)



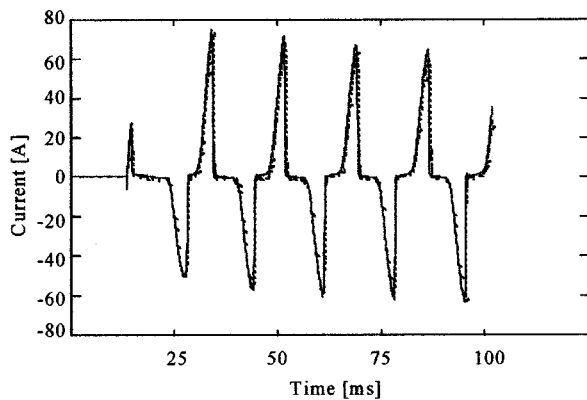
(b)

Fig. 4. Laboratory test data of ct saturation. (a) Ct saturation test without remanence in the ct core. (b) Ct saturation test with remanence in the ct core.

ondary side. The primary branch is negligible and could be ignored without sacrificing the accuracy of the results.



(a)



(b)

Fig. 5. Comparison of EMTP simulations and laboratory data. (a) Laboratory test with high ct secondary burden and without remanence in the ct [Fig. 4(a)], and EMTP simulation (solid line). (b) Laboratory test with high ct secondary burden and with remanence in the ct [Fig. 4(b)], and EMTP simulation (solid line).

B. Current Transformer Model Data

The following summarizes the procedure recommended to generate the necessary data to simulate the ct saturation cases using the EPRI/DCG EMTP (see the Appendix for EMTP files):

- 1) Use the subroutine CONVERT (for EMTP) or SATURATION (for ATP) to convert the ct saturation curve V_{rms} versus I_{rms} data to peak flux versus peak current.
- 2) Use the subroutine HYSDAT (for EMTP) or HYSTERESIS (for ATP) to generate the hysteretic reactor {type 96} data. The above subroutine requires the peak flux and peak current at the point where the hysteresis curve becomes single valued. This point was selected as the point where $I_e = 10.0$ A rms with a corresponding voltage of 175.0 V rms.
- 3) Modify the last data point of the hysteresis curve generated by EMTP or ATP subroutine to correct for the ct air-core reactance which can be calculated from the ct dimensions. The calculated air-core inductance from the ct dimensions is approximately 156.4 mH. The air-core reactance from the hysteresis curve is about 155.3 mH.
- 4) The current and voltage below which the magnetizing inductance was assumed to be linear were selected from the $V-I$ curve as $V_{\text{rms}} = 105.0$ V and $I_{\text{rms}} = 0.05$ A.

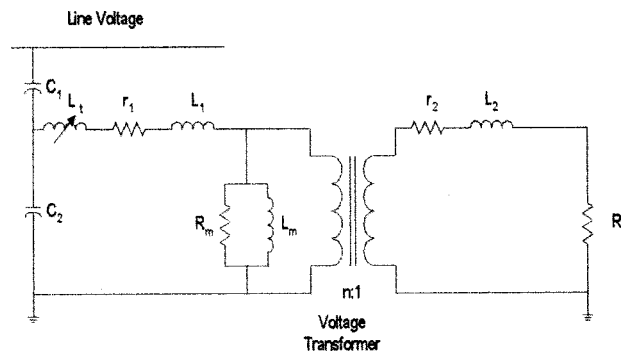


Fig. 6. Basic ccvt model with equivalent circuit of vt.

C. Ct Simulation Results

All four different core models investigated by the WG produced nearly identical results and the simulation results compared very well with the actual laboratory test data. The results shown in Fig. 5(a) and (b) can be regarded as typical output.

Fig. 4(a) and (b) show the primary and secondary ct currents scaled to the primary side obtained in the laboratory, while Fig. 5(a) and (b) show a comparison of the recorded laboratory secondary ct waveforms and the simulated secondary ct waveforms using the EPRI EMTP for the two cases. The first case results are quite satisfactory with the exception of a slightly larger magnitude negative loops. This is observed for all the core models. The EMTP hysteretic reactor (type 96) model was used since it allows inclusion of remnant flux in the ct core. The simulation results for the second case are nearly identical to the laboratory tests. The EMTP models used are shown in more detail in the Appendix.

The significant features that must be included in a ct model are:

- A good nonlinear core representation with ability of the model to accept initial core remanence. Representation of hysteresis is not as critical.
- The final slope of the hysteresis curve versus current, should be compared with the air-core reactance of the ct and should be adjusted accordingly. This assures a good transient performance of the model when compared to actual laboratory tests.

IV. CCVT MODEL

Fig. 6 shows the equivalent circuit of a ccvt. In order to avoid some of the insulation problems in a wound vt at high voltage levels, some of the step down ratio is achieved in a capacitive divider prior to applying the voltage to the voltage transformer. The capacitive voltage divider C_1 and C_2 brings the primary voltage down to $C_1 V / (C_1 + C_2)$ where V is the voltage applied to the divider. This voltage is then applied to the wound vt via a tuning reactor L_t and the output of the vt is connected to the burden. In many designs the tuning reactor is in the ground line rather than the high voltage lead of the vt but this does not affect the analysis and simulation results. The function of the tuning reactor is to minimize the equivalent source impedance at 60 Hz by tuning it to the capacitance $C_1 || C_2$ in order to allow the

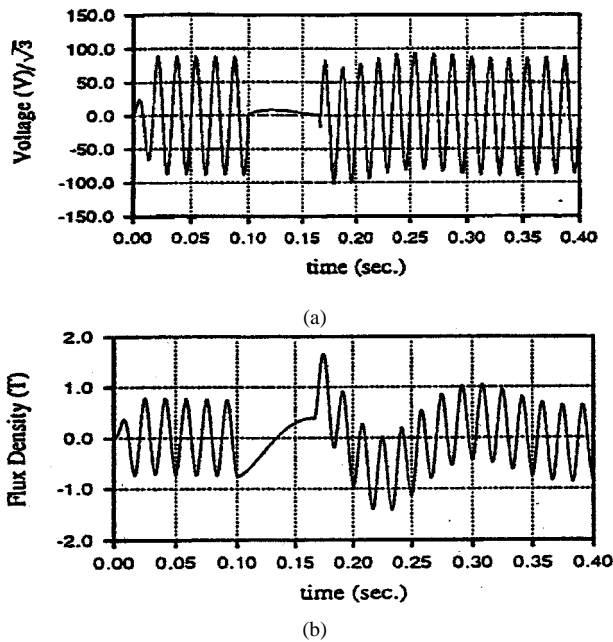


Fig. 7. (a) Secondary voltage for a reclose condition. (b) Core flux density for the case shown in Fig. 7(a).

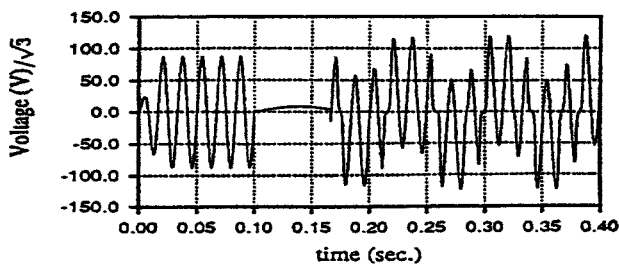


Fig. 8. Secondary voltage with light burden. (20 VA for a 200 VA ccvt).

burden to draw its current without causing significant voltage drop and thus affecting the accuracy of the measured voltage.

This feature was necessary when the instruments comprising the burden drew significant currents from the ccvt. The interaction of the source capacitance with the combined inductance of the tuning reactor L_t and the magnetizing inductance L_m of the voltage transformer is responsible for the subsidence transient problem and could lead to ferroresonance under particular excitation conditions. The elements shown in Fig. 6 are sufficient to describe the ccvt for frequencies up to 500 Hz. The major simulation challenge is the representation of the nonlinear elements in the magnetizing branch of the vt (L_m and its parallel resistance) since both vary with the excitation of the core.

Some authors have used nonlinear elements available in EMTF [2], [8] while others have used custom current source circuits (see Section II-B) which fit well into the Dommel algorithms [5]. The latter are particularly suitable for real time simulation when there is no time for iterations. Fig. 7(a) shows simulation of reclose operation from [5] for a case giving rise to a subsidence transient. (Note the absence of any high frequency oscillation at the voltage collapse due to the absence of stray capacitances in the model.) The burden in this case is the rated value of 200 VA. The transient can be seen much

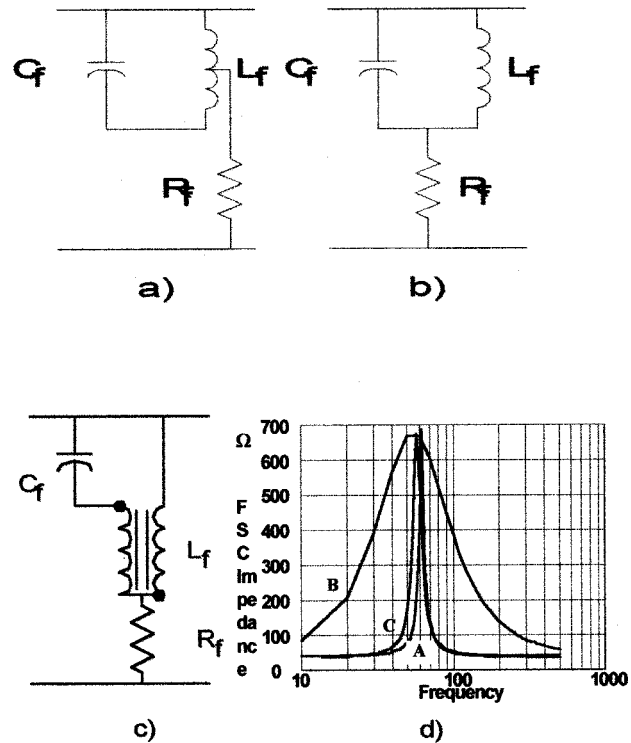


Fig. 9. Ferroresonance filter circuit: (a) actual design, (b), (c) digital models, and (d) frequency response of 9(a) (curve A), 9(b) (curve B), and 9(c) (curve C).

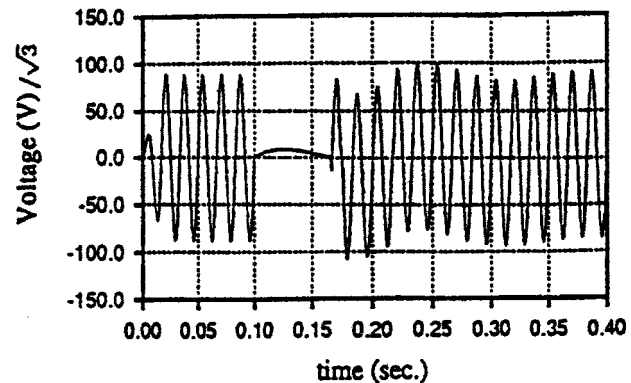


Fig. 10. Burden voltage for the case shown in Fig. 8 with ferroresonance filter in the current.

more clearly on the core flux waveform shown in Fig. 7(b). No ferroresonance occurs

This low frequency phenomenon can also give rise to ferroresonant conditions if the reclose occurs when the flux density is at or near saturation and the burden is very small (Fig. 8).

This case is for a light burden (20 VA for a 200 VA ccvt) condition [7]. Another condition known to give rise to ferroresonance is saturation of the auxiliary transformer in a relay input circuit which forms the burden of the ccvt [6]. As the auxiliary transformer comes out of saturation the sudden transition from a very low to a high impedance can, depending on the flux condition in the vt of the ccvt, give rise to ferroresonance. One of the early techniques used to avoid ferroresonance was to add

sufficient damping to the burden. A more sophisticated technique uses ferroresonance suppression circuits (FSC's) with a low impedance around the subsidence transient frequency to increase the damping at this frequency.

FSC can be designed in two operational modes: active and passive.

FSC's in an active operational mode consist of capacitors and iron core inductors connected in parallel and tuned to the fundamental frequency. They are permanently connected on the secondary side and affect the ccvt transient response.

FSC's in a passive operational mode consist of a resistor connected on the secondary side. This resistor can be permanently connected. Another option is to have a gap or an electronic circuit connected in series with the resistor, which are activated whenever an overvoltage occurs. This design avoids the loading effect of the FSC under normal conditions. These FSC's do not affect ccvt transient response unless an overvoltage occurs.

An active operational mode FSC design is shown in Fig. 9(a). Capacitor C_f is connected in parallel with an iron core inductor L_f tuned to the fundamental frequency. Resistor R_f is a damping resistor designed to damp ferroresonance oscillations within one cycle. The circuit is tuned with a high Q factor in order to attenuate ferroresonance oscillations at any frequency except the fundamental (Fig. 9(d), curve A).

The FSC can be modeled using two different L_f representations: FSC model with L_f represented as an air core inductance, as shown in Fig. 9(b). Components C_f and L_f are tuned to 60 Hz. This circuit has low Q factor as shown in Fig. 9(d), curve B. The FSC can also be modeled as shown in Fig. 9(c). L_f represented as a nonsaturable transformer. Primary and secondary windings are connected with polarities as presented in Fig. 9(c). The calculated L_f value is incorporated in the transformer model as a self inductance so that parallel resonance occurs at the fundamental frequency. At other frequencies, only the leakage inductance is involved and the damping resistor is the one which attenuates ferroresonance oscillations. This circuit has a high Q factor, very close to the actual design as shown in Fig. 9(d), curve C. FSC simulation using the transformer representation of L_f is more accurate [8]. Fig. 10 shows the effect this filter has on damping of the ferroresonance.

The equivalent circuit shown in Fig. 6 is not adequate for predicting the high frequency response of the ccvt. At frequencies around 1 kHz [6] it is necessary to consider the stray capacitances in the various circuit elements in order to explain the measured frequency responses in the linear region of operation [2]. Fig. 11 shows the influence of the coupling capacitor and stray capacitances on the frequency response for a typical ccvt.

Fig. 12 shows the equivalent circuit of a particular ccvt including stray capacitances. Fig. 13 shows the frequency response for the simulation model and the actual ccvt. The frequency response tests were conducted at low voltage levels and do not reveal any of the effects which result from vt core saturation, e.g., ferroresonance. The response does however reveal a rejection "cusp" around 1 kHz where the response falls off rapidly. The rejection cusp is almost entirely due to the parallel resonance of the compensating inductor and

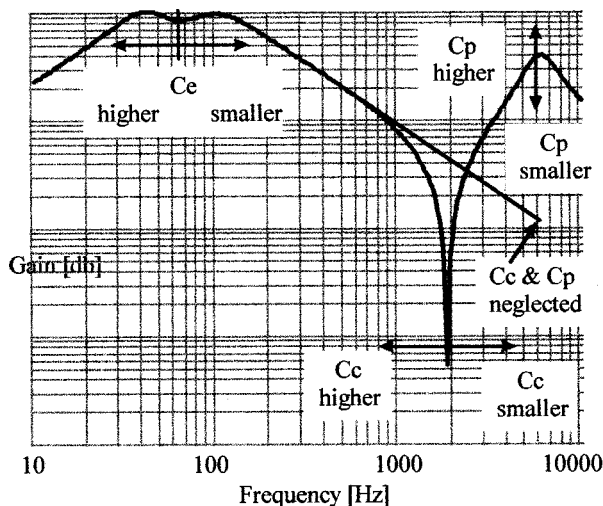


Fig. 11. Frequency response of ccvt in linear region.

its stray capacitance. The voltage across the compensating inductor at this frequency can be 7 to 8 times the normal 60 Hz value. If the line voltage input contains frequencies around this value, e.g., capacitor bank energization, it is important to model any spark gap across the tuning inductor which can fire and alter the frequency response under this resonant condition [6].

The significant features which must be included in the ccvt model are therefore:

- A good nonlinear core representation for any elements containing iron. The core model should at least be capable of accepting starting core remanence if it does not include hysteresis.
- Stray capacitance of the compensating inductor and the primary capacitance across the vt when the bandwidth of the relay under test extends beyond the rejection cusp frequency (typically >500 Hz).
- Proper modeling of any voltage limiting elements, e.g., spark gaps, saturating reactors or metal oxide varistors across the compensating inductor or ferroresonant filter.
- Proper modeling of the drain coil if it is part of the ccvt when the ccvt is used to couple a carrier signal on the power line in addition to providing voltage signals to protective relaying systems.

V. VOLTAGE TRANSFORMER MODEL

Modeling of magnetic voltage transformers is, in principal, similar to modeling any other instrument transformer. However, the large inductance of the primary winding and the importance of heavy saturation and hysteresis loop require special attention. Fig. 14 shows the needed model parameters to accurately simulate the transient response of vts.

A. Determination of Model Parameters from Tests and Manufacturer's Data Sheets

- R_{out} can be measured with a conventional, high accuracy Ohm-meter.

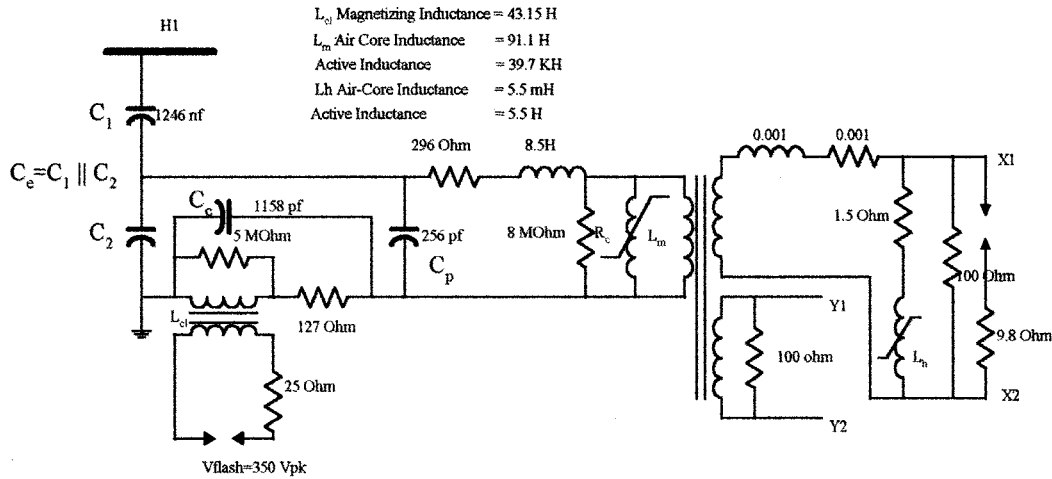


Fig. 12. Complete equivalent circuit of a 345 kV cvct.

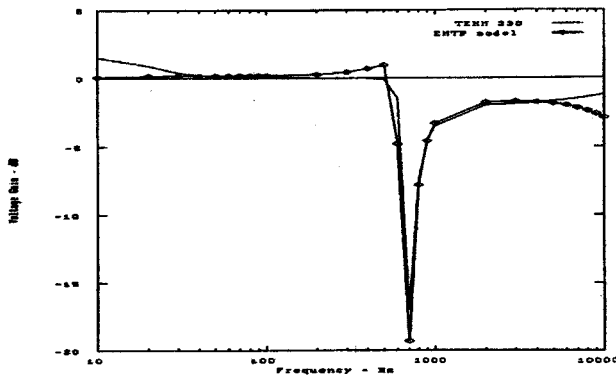


Fig. 13. Frequency response of cvct linear region.

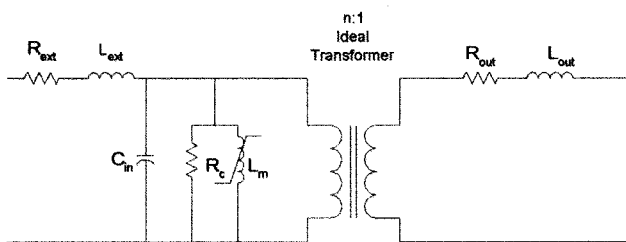


Fig. 14. Equivalent circuit of a vt with hysteric core.

- C_{in} can be determined from the manufacturer's data on capacitive current versus input voltage.
- R_{core} can be determined from the manufacturer's data on iron losses versus applied voltage.
- R_{ext} can be measured using a conventional Ohm-meter.

The most difficult elements to be determined are L_{out} , L_{ext} , and L_m the hysteric element. In particular, it is very difficult to separate the value of L_{ext} from the hysteric element L_m and a special measurement might be required to accomplish this task.

This special test is described below to help users obtain these parameters.

The primary of the vt is energized with a dc source of ~ 125 V to excite the core. This can take up to a few seconds. Then the primary of the vt is shorted out and the flux is allowed to decay. This can take up to tens of seconds. Next, the polarity of the dc source is reversed and the sequence is repeated. After several such sequences the core has reached a repeatable pattern of energizations/deenergizations. The waveshapes of primary voltage, primary current, and secondary voltage are recorded during each sequence. From these waveshapes a flux-current hysteric function can be generated. The magnetic flux can be obtained by numerically integrating the input voltage wave as $\Psi_m = \int V dt = \Sigma V \Delta t$, where Δt is the sampling time of the waveform. The parameter L_{ext} can be determined as the slope of Ψ_m curve at the maximum current. If the input current is not enough to drive the vt into heavy saturation this test could be repeated with higher dc voltage with the help of a capacitor, rather than a permanent dc source. The capacitor is first charged and then discharged through the primary of the vt. This is a transient way of testing which eliminates the steady state heating of the vt primary winding, which could be substantial if a permanent dc source is used for testing. As an example, the value of L_{ext} was determined to be around 38.5 Henry for a commercial 34.5 kV/115 V vt.

VI. CONCLUSIONS

This paper has investigated a number of mathematical models that could be used to represent the nonlinear behavior of the magnetic core of instrument transformers.

The Working Group compared the results of the four mathematical models of cts with actual laboratory saturation test data and the results of all four models were almost identical and in extremely good agreement with the laboratory test data.

The most significant features that the instrument transformer models must include, have been described in the paper in great detail.

It is imperative that relay systems be tested under transient conditions in order to assure a high degree of dependability and security in their design and applications. The use of electromagnetic transient programs to adequately model the different power system components and to generate transient data to assess the performance and correct application of modern static and microprocessor high-speed protective relays has become essential.

APPENDIX
EMTP MODEL SETUP FOR CT SATURATION

A. CT and Secondary Burden Data

Turns Ratio	900/5	
Mean Core Length	0.4987	meters
Area	$1.91532E-3$	square meters
Winding Resistance	0.253	Ohms
Remnant Flux	0.4645	Volt-s
Burden (case 1)	$1.30 + j0.175$	Ohms
Burden (case 2)	$8.33 + j0.175$	Ohms

B. CT Saturation Data

I_{rms} (Amps)	V_{rms} (Volts)
$40.0E-3$	85.0
$50.0E-3$	105.0
$100.0E-3$	140.0
$200.0E-3$	150.0
$10000.0E-3$	175.0
9999	

C. EMTP Subroutine CONVERT

```

C =====
C WRITTEN BY Demetrios A. Tziouvaras
C =====
BEGIN NEW DATA CASE
SATURATION
C
C CONVERSION OF V-I CHARACTERISTIC
C TO PEAK FLUX VS PEAK CURRENT 900/5
C C-100 BUSHING CURRENT TRANSFORMER
C SQUARE D ARMCO M4 GRAIN ORIENTED
C
C FOR THE EMTP TO ACCEPT VOLTAGE IN VOLTS AND
C CURRENT IN AMPS
    
```

```

C WE MUST SET VBASE = 1.0*E-3 AND PBASE =
1.0*E-6
C
C FREQU] [ VBASE] [PBASE ] [IPUNCH] [KTHIRD]
60.0 1.0e-3 1.0e-6 0 0
C
C IRMS AMPS ] VRMS ]
40.0E-3 85.0
50.0E-3 105.0
100.0E-3 140.0
200.0E-3 150.0
1000.0E-3 160.0
10000.0E-3 175.0
9999
BLANK CARD ENDING CASE
BLANK
    
```

D. EMTP Output from CONVERT Subroutine

I_{peak} (Amps)	Flux peak (Volts-s)
$.56568542E-01$	$.31886203E+00$
$.71508353E-01$	$.39388839E+00$
$.17030469E+00$	$.52518452E+00$
$.47571570E+00$	$.56269770E+00$
$.23289864E+02$	$.65648065E+00$
9999	

E. EMTP Subroutine HYSDAT

```

C =====
C WRITTEN BY Demetrios A. Tziouvaras
C =====
BEGIN NEW DATA CASE
SATURATION
C
C V-I CONVERSION TO TYPE-96 HYSTERETIC IN-
DUCTOR
C USE THE LAST ROW OF DATA FROM THE CONVERT
C ROUTINE PUNCHED OUTPUT
C
C FREQ ]
88.
C ITYPE] [ LEVEL] [IPUNCH]
1 4 0
C
C I SAT] [F SAT ]
C
23.28986.6564807
BLANK CARD ENDING CASE
BLANK
BEGIN NEW DATA CASE
    
```

F. EMTP Output from Hysdat Subroutine

I_{peak} (Amps)	Flux peak (Volt-s)
-.873 369 77E + 01	-.641 034 11E + 00
-.582 246 50E + 01	-.637 172 44E + 00
-.262 010 93E + 01	-.623 656 65E + 00
-.116 449 30E + 01	-.610 140 89E + 00
-.436 684 86E + 00	-.598 555 93E + 00
.145 561 62E + 00	-.575 386 01E + 00
.509 465 68E + 00	-.548 354 46E + 00
.844 257 39E + 00	-.502 014 65E + 00
.101 893 14E + 01	-.424 781 63E + 00
.116 449 30E + 01	-.308 932 09E + 00
.145 561 63E + 01	.206 598 33E + 00
.160 117 78E + 01	.285 762 19E + 00
.203 786 27E + 01	.386 165 12E + 00
.262 010 93E + 01	.463 398 14E + 00
.317 324 33E + 01	.502 014 65E + 00
.414 850 62E + 01	.540 631 16E + 00
.567 690 31E + 01	.575 386 01E + 00
.778 754 72E + 01	.602 417 60E + 00
.101 893 13E + 02	.621 725 85E + 00
.145 561 62E + 02	.641 034 11E + 00
.232 898 60E + 02	.656 480 70E + 00
C .320 235 58E + 02	.660 342 37E + 00
.397 625 71E + 03	.714 626 08E + 00
.999 900 00E + 04	

Notes:

- 1) The final slope of the data from the subroutine HYSDAT was modified to the slope of the calculated air-core inductance of the ct. The commented line with a C is the actual HYSDAT data as compared with the data from the line which follows which reflects the calculated ct air-core inductance.

- 2) The residual flux was calculated from the final hysteresis data points:

$$\text{residual flux} = 65.0\% * .714\ 620\ 8\ \text{V-s.}$$

REFERENCES

- [1] W. L. A. Neves and H. W. Dommel, "On modeling iron core nonlinearities," *IEEE Trans. on Power Systems*, vol. 8, no. 2, pp. 417-423, May 1993.
- [2] M. Kezunovic, C. W. Fromen, S. L. Nilson, L. Kojovic, V. Skendzic, and D. R. Sevcik, "Digital models of coupling capacitor voltage transformers for protective relay transient studies," *IEEE Trans. on Power Delivery*, vol. 7, no. 4, p. 1927, Oct. 1992.
- [3] H. W. Dommel, "Digital computer solution of electromagnetic transients in single and multiphase networks," *IEEE Trans. on PAS*, vol. PAS 88, no. 4, p. 388, Apr. 1969.
- [4] J. R. Lucas, "Representation of magnetization curves over a wide region using non-integer power series," *IJEEE*, vol. 25, no. 4, p. 335, 1988.
- [5] J. R. Lucas, P. G. McLaren, and R. P. Jayasinghe, "Improved simulation models for current and voltage transformers in relay studies," *IEEE Trans. on Power Delivery*, vol. 7, no. 1, p. 152, Jan. 1992.
- [6] M. J. Wiseman, "CVT transient behavior during shunt capacitor switching," Ontario Hydro Study no. W401, Apr. 15, 1993.
- [7] P. G. McLaren, J. R. Lucas, and W. W. L. Keerthipala, "A digital simulation model for a ccvt in relay studies," in *IPEC '93*, Singapore, Mar. 1993.
- [8] Lj. A. Kojovic, M. Kezunovic, and S. L. Nilsson, "Computer simulation of a ferroresonance suppression circuit for digital modeling of coupling capacitor voltage transformers," in *ISMM International Conference*, Orlando, FL, 1992.
- [9] D. C. Jiles and D. L. Atherton, "Theory of ferromagnetic hysteresis," *Journal of Magnetism and Magnetic Materials*, vol. 61, pp. 48-60, 1986.
- [10] D. C. Jiles, J. B. Thoeke, and M. K. Devine, "Numerical determination of hysteresis parameters for modeling of magnetic properties using the theory of ferromagnetic hysteresis," *IEEE Transactions on Magnetics*, vol. 28, no. 1, pp. 27-34, Jan. 1992.
- [11] R. Garret, W. C. Kotheimer, and S. E. Zocholl, "Computer simulation of current transformers and relays," in *41st Annual Conference for Protective Relay Engineers*, Apr. 18-20, 1988, Texas A&M University.
- [12] M. Kezunovic, L. J. Kojovic, A. Abur, C. W. Fromen, D. R. Sevcik, and F. Phillips, "Experimental evaluation of EMTP-based current transformer models for protective relay transient study," *IEEE Trans. on Power Delivery*, vol. 9, no. 1, pp. 405-412, Jan. 1994.